


國立交通大學

電子物理研究所

碩士論文

碲化鎘膠體量子點之能量共振轉移



Resonant Energy Transfer of
CdTe Colloidal Quantum Dots

研究生：王威智

指導教授：周武清 教授

中華民國九十八年六月

碲化鎘膠體量子點之能量共振轉移

**Resonant Energy Transfer of
CdTe Colloidal Quantum Dots**

研究生：王威智

Student : Wei-Jhih Wang

指導教授：周武清 教授

Advisor : Prof. Wu-Ching Chou

國立交通大學

電子物理研究所

碩士論文

A Thesis

Submitted to Institute of Electrophysics
College of Science
National Chiao Tung University
in partial Fulfillment of the Requirements
for the Degree of Master
in
Electrophysics
June 2009
Hsinchu, Taiwan, Republic of China

中華民國九十八年六月

碲化鎘膠體量子點之能量共振轉移

研究生：王威智

指導教授：周武清 教授

國立交通大學電子物理研究所

中文摘要

我們利用光激螢光及時間解析光頻譜技術來分析單一尺寸(5.1 奈米)與混合兩種尺寸(3.4 和 5.1 奈米)的水溶性碲化鎘量子點之 Förster 能量共振轉移。

在單一尺寸樣品中，我們觀察到量子點薄膜之光激螢光能量相較於水溶液有一個紅移的現象。我們也利用時間解析光譜分析載子的複合機制，發現載子的生命期會隨著不同量子點尺寸而改變。綜合以上討論可證實載子以非輻射性的方式將能量從小的量子點轉移到大的量子點。並且發現能量紅移與樣品的尺寸分佈有關。

我們將兩種不同尺寸的量子點混和。從光激螢光光譜上可以觀察到小量子點的螢光強度受到抑制，伴隨著大量子點的螢光強度增強，這是由於小量子點的放射光譜與大量子點的吸收光譜之間的重疊增加，導致量子點之間的偶極交互作用力增強，造成明顯且有效率的能量轉移。

最後，我們發現對於能量轉移的效率而言，小量子點與大量子點的混和濃度比例會是一個很重要的影響因素。當小量子點與大量子點的混和比例越大，大量子點充分地被小量子點包圍，提升小量子點的能量轉移效率。小量子點的數量持續增加，大量子點的比例相對減少，此時小量子點的載子複合機制將不受到大量子點的影響。

Resonant Energy Transfer of CdTe Colloidal Quantum Dots

Student : Wei-Jhih Wang

Advisor : Prof. Wu-Ching Chou

**Institute of Electrophysics
National Chiao Tung University**

Abstract

The dynamics of Förster resonance energy transfer (FRET) in mono-dispersed (5.1 nm) and mixed-size (50 % 3.4 nm and 50 % 5.1 nm) water-soluble CdTe quantum dots (QDs) were studied by using photoluminescence (PL) and time-resolved PL (TRPL) spectroscopy.

A significant PL energy red-shift was observed for the mono-dispersed CdTe colloidal QDs films when compared with that of the mono-dispersed CdTe colloidal QDs solutions. The energy dependent TRPL spectra directly reveal the energy transfer from small to large QDs. We found that the amount of PL energy red-shift is independent of CdTe QDs' size but depends on the PL line-width.

To study the effect the spectral overlap of donor emission and acceptor absorption on the FRET efficiency, a mixture of two different sizes CdTe QDs (50 % 3.4 nm and 50 % 5.1 nm) was studied. The quenching/enhancement of PL intensity and lifetime of donors/acceptors are evidences of FRET effect in mixed-size water-soluble CdTe QDs.

Furthermore, the donor to acceptor concentration ratio in the mixed-size CdTe QDs films is an important parameter to influence the FRET efficiency. As the ratio is increased, the

FRET rate and the efficiency is firstly enhanced and then decreased. It is due to the fact that acceptors are surrounded by more and more donors in the beginning. However, the relative amount of available acceptors is decreased if the ratio is further increased.



Acknowledgement

研究所的兩年過得還真快，轉眼間就要畢業了。在交大短短的兩年時間內，我遇到了各式各樣的人事物，也學習到許許多多難得的經驗，雖然在研究的過程中遇到了不少阻礙我前進的絆腳石，但是在朋友及家人的鼓勵與支持下，我走過來了。在畢業的前夕，我坐在研究室裡回憶這兩年，心中的感動真是難以言語。

這段時間，我首先要感謝我的指導教授周武清博士，感謝您當年願意讓我加入奈米科技實驗室這個大家庭，每次咪廳的時候，您不僅會給予我們學術上的建議，也教導我們不論是現在或是以後都該有的做人處事的道理。還要感謝褚德三教授、楊賜麟教授、張恆雄教授以及沈志霖教授，感謝各位教授給予我研究上的意見。再來我要特別感謝彥丞學長，學長的研究精神及實驗的敏銳度、細心度都讓我十分欽佩，在學長的帶領下我才能夠順利畢業，也恭喜學長在今年得到了博士學位！還要感謝實驗室的各位學長姐妹們，感謝狗哥、龜泰、崑峯、瑞雯、惠琳、昱璇、李寧和溫博，有了你們的陪伴跟支持，我才能夠有個多采多姿的研究生生活。感謝狗哥在我一進實驗室就很照顧我，雖然你的聲音很大，但是卻很親切，先預祝狗哥明年可以順利畢業啦！也要感謝崑峯學長對我的照顧，每當我有研究或是生活上的問題時，你都能耐心分析給我聽並給予我建議，之前腳踝扭傷事件，你還真是讓我感動耶！還要感謝畢業的繼祖學長在口試那天特別回來給我支持，你的演講風格讓我十分欽佩，也一直是我的學習的目標。另外我還要感謝鏡學、富凱和俊榮，你們讓實驗室充滿歡樂，我們都很懷念你們，在這也祝福鏡學能順利拿到博士學位，富凱能早日賺大錢，恭喜俊榮年紀輕輕就當上老師耶！

最後，我要感謝我的家人，爸爸、媽媽、姐姐、妹妹以及小成員咪魯，感謝你們一路上的支持，特別要謝謝我最親愛的媽媽，謝謝您從我小時候就不斷栽培我、體諒我，凡事都為我著想，並教導我許多做人做事的道理。也要謝謝我的姐姐，家裡的大小事都是靠妳在幫忙打理，妳一定要健健康康的喔！我還要感謝我的女朋友 舒洵，在我大學時期就支持我到現在，這段時間謝謝妳的寬容及體諒，妳的鼓勵跟支持一直是我前進的動力。有了你們的支持，我才能完成我的碩士學位，這個學位、這份榮耀是屬於你們的！

Contents

Abstract (Chinese version)	<i>i</i>
Abstract (English version)	<i>ii</i>
Acknowledgement	<i>iv</i>
Contents	<i>v</i>
List of Figures	<i>vi</i>
List of Tables	<i>ix</i>
Chapter 1. Introduction	<i>1</i>
1.1 Colloidal Quantum Dots	<i>1</i>
1.2 Förster Resonance Energy Transfer (FRET)	<i>2</i>
1.3 Motivation	<i>4</i>
Chapter 2. Experimental Setup	<i>6</i>
2.1 Micro-Photoluminescence System	<i>6</i>
2.2 Time-Resolved Photoluminescence System	<i>7</i>
Chapter 3. Results and Discussion	<i>10</i>
3.1 FRET in Mono-Dispersed CdTe Colloidal Quantum Dots	<i>10</i>
3.2 FRET in Mixed-Size CdTe Colloidal Quantum Dots	<i>13</i>
3.2.1 Effect of the Spectral Overlap	<i>13</i>
3.2.2 Effect of the Concentration Ratio of Donor to Acceptor	<i>15</i>
Chapter 4. Conclusions	<i>33</i>
References	<i>34</i>

List of Figures

FIG. 2.1.	The experimental setup of PL system.	8
FIG. 2.2.	The experimental setup of TRPL system.	9
FIG. 3.1.	(a) Absorption and normalized PL spectra of mono-dispersed 5.1 nm CdTe QDs solution at room temperature. (b) Normalized PL spectra of 5.1 nm mono-dispersed CdTe QDs solution (red line) and film (black line).	20
FIG. 3.2.	(a) Normalized PL spectra of diluted CdTe QDs solution (red line) and film (black line). (b) Schematic draw of radiative energy transfer. (c) PL decay curves of diluted film (black line) and dense film (red line) measured at 734 nm.	21
FIG. 3.3.	(a) Normalized PL spectra of mono-dispersed 5.1 nm CdTe QDs solution (red line) and film (black line). (b) TRPL spectrum of 5.1 nm CdTe QDs solution recorded at 734 nm is also displayed.	22
FIG. 3.4.	Instantaneous PL spectra of the mono-dispersed 5.1 nm CdTe QDs film.	23
FIG. 3.5.	Dynamic red-shift of the PL peak emission of the mono-dispersed 5.1 nm CdTe QDs film.	24
FIG. 3.6.	The amount of red-shift versus FWHM for 2.3 nm (square), 3.4 nm (circle), 5.1	

nm (triangle) CdTe QDs size. 25

FIG. 3.7. (a) Absorption (dash line) and normalized PL spectra (solid line) for mono-dispersed 2.3 nm (blue line), 3.4 nm (green line) and 5.1 nm (red line) CdTe QDs solution at room temperature. (b) PL spectra for film of 3.4 nm (green line), 5.1 nm (red line), and mixture of the two (black line). 26

FIG. 3.8. (a) PL decay curves of the pure 3.4 nm CdTe QDs film (green line) and the mixed-size CdTe QDs film (black line) measured at 635 nm. (b) PL decay curves of the pure 5.1 nm CdTe QDs film (red line) and the mixed-size CdTe QDs film (black line) measured at 734 nm. 27

FIG. 3.9. True-color images of the pure donors, pure acceptors, and mixed CdTe QDs in solutions and films. 28

FIG. 3.10. (a) PL spectra of mixed-size CdTe QDs solutions with different donor to acceptor concentration ratios ($D/A = 1, 3, \text{ and } 5$). (b) PL spectra of mixed-size CdTe QDs films with different donor to acceptor concentration ratios ($D/A = 1, 3, \text{ and } 5$). 29

FIG. 3.11. (a) PL decay curves of donors detected at 635 nm in the mixed CdTe QDs films with different D/A ratios. (b) PL decay curves of acceptors detected at 734 nm in the mixed CdTe QDs films with different D/A ratios. The inset shows the initial PL decay curves of acceptors. 30

FIG. 3.12. (a) TRPL image of mixed-size CdTe QDs film ($D/A = 5$). (b) Temporal evolution

of PL spectra of mixed-size CdTe QDs film ($D/A = 5$). **31**

FIG. 3.13. (a) TRPL spectra of donors in mixed-size CdTe QDs films detected at 635 nm for $D/A = 5, 6, 8,$ and 9 . (b) Average PL lifetime of donors (open circles) recorded at peak position in the mixed-size CdTe QDs films as a function of D/A ratios. The PL lifetime of pure donors is also shown (red dash line). **32**



List of Tables

Table 3.1 FWHM for 2.3 nm, 3.4 nm, and 5.1 nm CdTe QDs solution, and the amount of red-shift for 2.3 nm, 3.4 nm, and 5.1 nm CdTe QDs film. **18**

Table 3.2 Amount of spectra overlap, FRET efficiency, FRET rate, Förster critical radius, and the distance between donor and acceptor for the mixture of two QDs size (3.4 nm + 5.1 nm and 2.3 nm + 3.4 nm). **19**



Chapter 1. Introduction

This thesis studies the Förster resonance energy transfer in water-soluble CdTe colloidal quantum dots (QDs) by using the photoluminescence (PL) and time-resolved PL (TRPL) spectroscopy. Chapter 1 introduces the optical characteristics and potential applications of colloidal QDs (Section 1.1). The Förster resonance energy transfer (FRET), which is a non-radiative dipole-dipole coupling mechanism, is discussed (Section 1.2). The motivation of this study is also illustrated (Section 1.3). Chapter 2 describes the experimental methods used in this study. Chapter 3 discusses the FRET mechanism in mono-dispersed and mixed-size CdTe QDs films. Finally, Chapter 4 summarizes this thesis.

1.1 Colloidal Quantum Dots

Chemically synthesized semiconductor nanocrystals (NCs) or colloidal quantum dots (QDs) have been studied extensively over the past few years. In QDs, the charge carriers confined to three dimensions resulting atomic-like electronic energy levels [1]. It is possible to change their electronic and optical characteristics via tuning their chemical composition, shapes, and sizes. As the dot size is reduced, the emission energy of QD shifts to high energy due to quantum confinement effect [2]. Besides, QDs exhibit of high PL quantum yield (PLQY). Y. He *et al.* have synthesized high-quality CdTe nanocrystals in aqueous phase by utilizing illumination methods and the PLQY reaches 98% [3]. Based on tunable band gap and efficient quantum yield of QDs, they are potential candidates for optoelectronics [4-7]. Furthermore, the photostability of colloidal QDs is higher than classical fluorescence dye markers [8], colloidal QDs are used to replace fluorophores or dyes for use in biolabeling and biosensing [9].

1.2 Förster Resonance Energy Transfer (FRET)

Förster resonance energy transfer (FRET) is a non-radiative dipole-dipole coupling mechanism, which occurs not only between a molecular pairs or organic dyes but also between semiconductor QDs. The mechanism governed to a large extent by spectral overlap between the normalized emission spectrum of small dots (donors) and absorption spectrum of large dots (acceptors), as well as by the spatial distance between donors and acceptors. According to the Förster theory, the energy transfer rate is given by [10]

$$k_T(r) = \frac{1}{\tau_D} \left(\frac{R_0}{R_{DA}} \right)^6, \quad (1)$$

where τ_D is the lifetime of the donor in the absence of the acceptor and R_{DA} is the distance between the donor and acceptor. R_0 denotes the Förster critical radius at which the energy transfer efficiency is 50%. The Förster critical radius depends on the overlap between normalized emission spectrum of donor and absorption spectrum of acceptor. Generally, R_0 is in the range of 15 – 60 Å [11]. R_0 is given by the following equation

$$R_0 = 0.2108[\kappa^2 n^{-4} \phi_{donor} J(\lambda)]^{1/6} (\text{Å}), \quad (2)$$

where κ^2 is the dipole orientation factor and ranges from 0 to 4, n is the refractive index of medium, ϕ_{donor} is the PL quantum yield of donor in the absence of acceptor, and $J(\lambda)$ is the integral spectral overlap between the absorption peak of acceptor and emission peak of donor. $J(\lambda)$ is described as follows

$$J(\lambda) = \int_0^\infty F_D(\lambda) \varepsilon_A(\lambda) \lambda^4 d\lambda, \quad (3)$$

where $F_D(\lambda)$ is the normalized emission spectral of donor and $\varepsilon_A(\lambda)$ is the absorption coefficient of the acceptor. The FRET efficiency (η) is accounted for the fraction of excitations transferred from donors to acceptors and is defined as

$$\eta = \frac{k_T}{k_D + k_T} = \frac{k_T}{1/\tau_D + k_T}, \quad (4)$$

Using Eqs. (1), the FRET efficiency can be related to the ratio r/R_0 :

$$\eta = \frac{1}{1 + (R_{DA}/R_0)^6}. \quad (5)$$

The FRET efficiency can also obtain from the PL lifetime and PL intensity of the donor, which are given by [12]

$$\eta = 1 - \frac{\tau_M}{\tau_D}, \quad (6)$$

$$\eta = 1 - \frac{F_M}{F_D}, \quad (7)$$

where τ_M and τ_D are the PL lifetime of the donor mixed with acceptors and that of pure donor, respectively. F_M and F_D are the PL integral intensity of the donor mixed with acceptors and that of pure donor, respectively.

Recently, the FRET process between semiconductor QDs has been investigated in closely packed mixed layers and in separated donor and acceptor layers [13-16]. Feldmann's group has demonstrated a cascaded FRET in artificial solids formed by layers of QDs [17]. Efforts to improve the FRET process have been focused on structures with reduced donor-acceptor QDs' separation, improved spectral overlap of the donor emission and acceptor absorption spectra, and increased packing density of the layers. Achermann *et al.* have proposed a method to inject excitons from InGaN quantum well into CdSe/ZnS colloidal QDs indirectly via FRET process. This approach can eliminate the limitation of colloidal QDs for applications in optoelectronics because the electrical pumping is designed on InGaN quantum well. They found that the transfer efficiency is greater than 50 percent [18].

1.3 Motivation

The FRET-related studies, in the past few decades, are all focused on CdSe QDs [19-22]. However, CdSe/ZnS QDs cannot be directly used in biological applications due to their hydrophobic character. A general approach is to transfer the hydrophobic QDs from the organic phase to aqueous solution by wrapping an amphiphilic polymer around the particles [23]. Although this method is efficient, it is relatively complicated. Another effective approach is to substitute the hydrophilic molecules, which have strong polar groups such as carboxylic acid or reactive groups such as Si-O-R, for surface-binding TOPO [24]. However, the PLQY of the CdSe QDs decreases rapidly when the QDs are transferred into water.

Recently, CdTe QDs have attracted much attention because their emission wavelength can reach near-infrared (better penetrability) range and the QDs exhibit high PL quantum yield. Most importantly, they are water soluble and can be directly synthesized in aqueous solution. Therefore, CdTe QDs possess potential for using in biology and optoelectronics. FRET-related studies in CdTe QDs are recently of increasing interest in both physics and biology research activities. However, studies on FRET mechanism of mono-dispersed and mixed-size CdTe QDs still lack in the literature. Xu *et al.* investigated FRET between CdTe QDs during the evaporation of the solvent using only PL measurement [25-26]. From the PL spectra, they found that the integral PL intensity of small dots decrease sharply while that of the large dots increase only slightly. It implies that the transfer efficiency is quite low and the FRET process cannot be fully supported in this case due to the lack of TRPL results.

In this thesis, we study the Förster resonance energy transfer in mono-dispersed and mixed-size CdTe QDs films by using PL and TRPL measurements. In order to shorten the inter-dot distance, CdTe QDs were drop cast onto glass slide from aqueous solution. After evaporation, the CdTe QDs deposited on the glass slide and formed a close-packed solid state film. To study the effect the spectral overlap of donor emission and acceptor absorption on the

FRET efficiency, a mixture of two different sizes CdTe QDs (50 % 3.4 nm and 50 % 5.1 nm) was studied. We also found that the donor to acceptor concentration ratio in the mixed-size CdTe QDs films is an important parameter to influence the FRET efficiency.



Chapter 2. Experimental Setup

In this chapter, we will introduce the experimental systems used in this thesis. The experimental systems include micro-photoluminescence (μ -PL) system and time-resolved photoluminescence (TRPL) system.

2.1 *Micro-Photoluminescence System*

The experimental setup of the μ -PL system is shown in Figure 2.1. The samples were deposited on a glass slide and loaded on the stage of microscope. The GaN pulsed diode laser (405 nm) was used as an excitation source at room temperature. An incident beam from a diode laser was focused to about $5 \mu\text{m}$ in diameter on the sample using a 20x long-working-distance ($\sim 20 \text{ mm}$) microscope objective. The PL signal was collected by the same microscope objective and guided to an optical fiber. The 415 nm edge filter was utilized to filter out the incident laser light. The iHR550 spectrometer, which is equipped with a multichannel LN_2 -cooled charge-coupled device (CCD), was used to analyze the PL spectra. The spectrometer is controlled by a computer which is also used to store and plot the collected data.

2.2 Time-Resolved Photoluminescence System

The experimental setup of TRPL system is similar to the PL system and shown in Figure 2.2. The only differences are: (1) the trigger from the pulsed laser diode is used to define the start ($t = 0$) of decay profile, (2) a high speed PMT instead of CCD is used to detect the PL signal. The diode laser produces light pulses with a repetition rate of 2.5 MHz. The signals were further analyzed by a Time Harp counting card, which was triggered with a signal from the diode laser. The decay traces were recorded using the time-correlated single photon counting technique (Time-Harp, PicoQuant). The overall temporal resolution is around 400 ps.



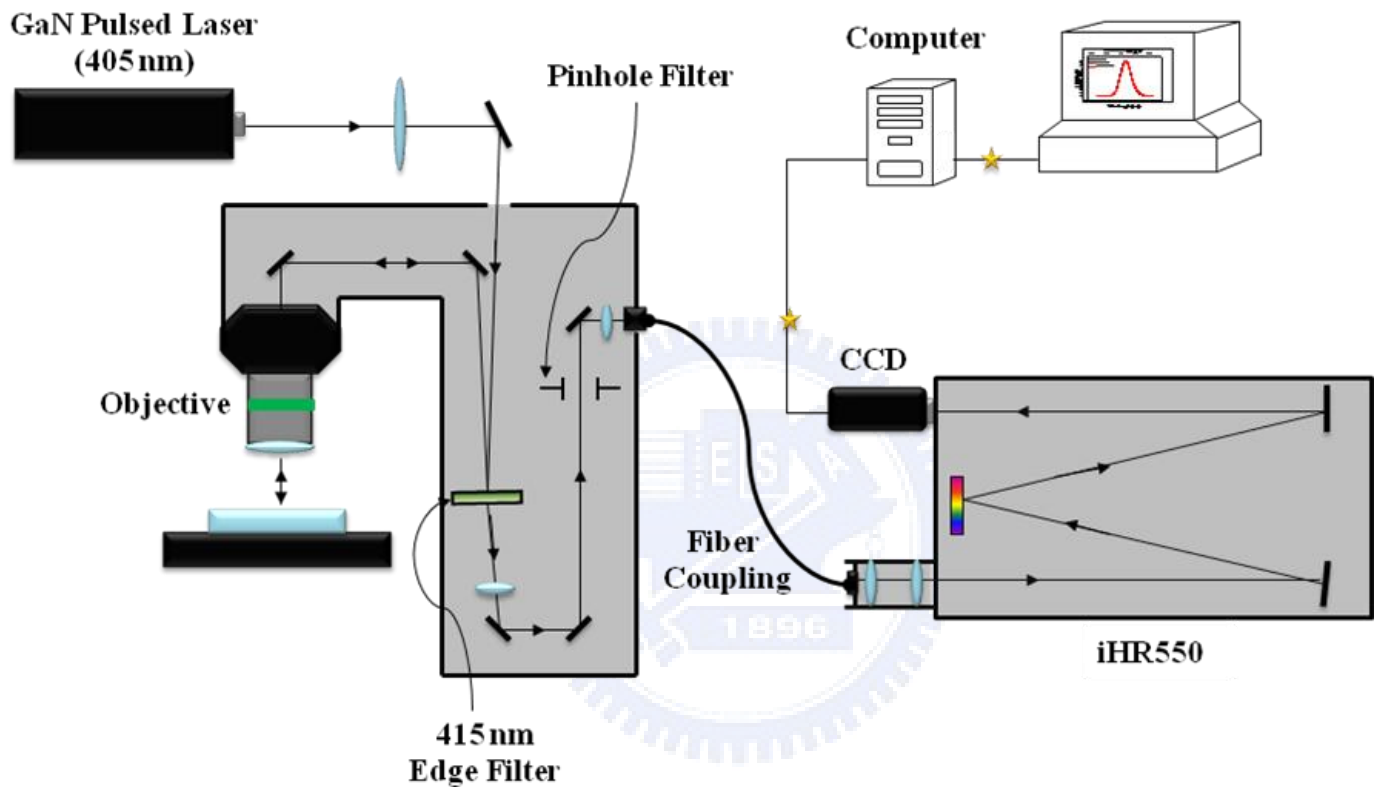


Fig. 2.1. The experimental setup of PL system.

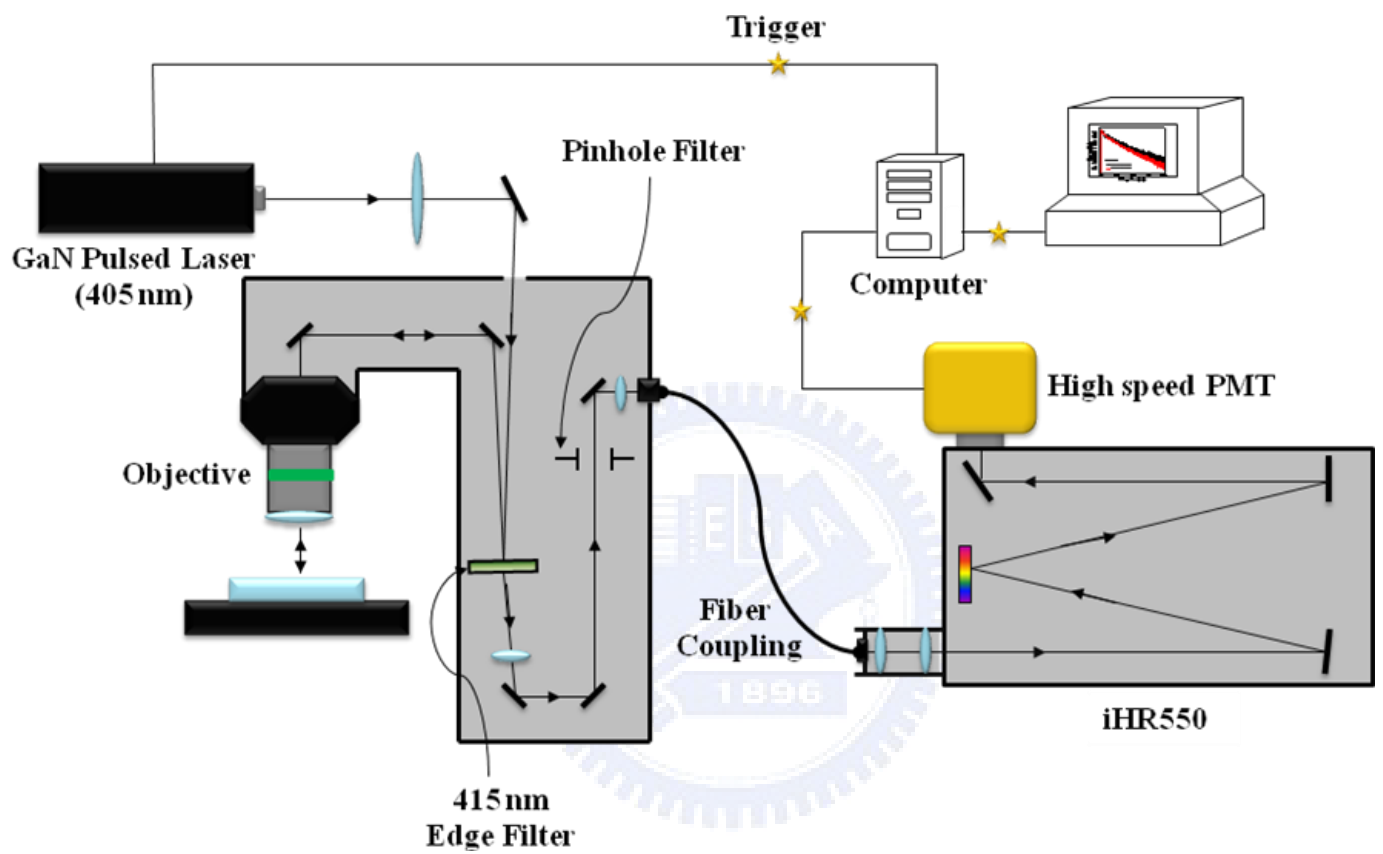


Fig. 2.2. The experimental setup of TRPL system.

Chapter 3. Results and Discussion

In this chapter, we study the FRET dynamics in close-packed CdTe colloidal QDs films via PL and TRPL measurements. In Section 3.1, the FRET mechanism in mono-dispersed CdTe colloidal QDs films will be discussed. In Section 3.2, we discuss the FRET mechanism in mixed-size CdTe QDs films. In addition, the FRET of the mixed-size CdTe QDs films with different donor to acceptor concentration ratios will also be investigated.

3.1 FRET in Mono-Dispersed CdTe Colloidal Quantum Dots

Figure 3.1(a) shows PL emission and absorption spectra of mono-dispersed CdTe QDs ($D = 5.1$ nm) solution (1.0×10^{-5} M). The PL emission peak is situated at ~ 719 nm. The CdTe QDs were then drop cast onto glass slide from aqueous solution. After evaporation, the CdTe QDs deposited on the glass slide and formed a close-packed solid state film. Figure 3.1(b) displays the PL spectra of 5.1 nm mono-dispersed CdTe QDs solution and film. An energy red-shift of about 40 meV can be observed for the QDs film. This energy red-shift could be caused by (1) the change of QDs' surface environment (oxidation) and (2) energy transfer among QDs. In the case of (2) energy transfer among QDs, the red-shift should be influenced by the inter-dot distance. On the other hand, the change of surface environment (oxidation) is not sensitive to the inter-dot distance. In order to identify the origin of the energy red-shift, a diluted CdTe QDs solution (1.0×10^{-7} M) was prepared and drop cast onto glass slide. Figure 3.2(a) shows the PL spectra of diluted CdTe QDs solution and film. We found that indeed the profile and the peak position of the normalized PL spectra remain the same as shown in Figure 3.2(a). Thus, we conclude that such a large energy red-shift in the close-packed film is attributed to the existence of energy transfer.

Energy transfer, including radiative energy transfer and non-radiative energy transfer, strongly depends on the inter-dot distance. Radiative energy transfer is a two step process

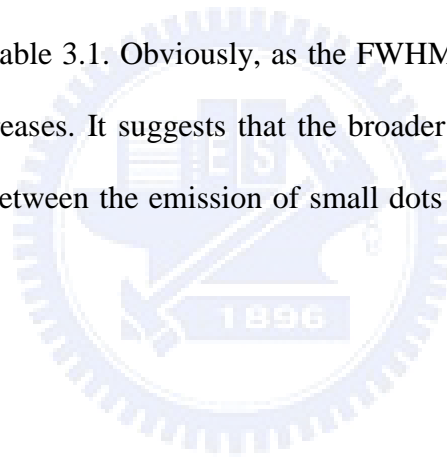
(see Figure 3.2(b)): a photon emitted by a donor is absorbed by an acceptor (reabsorption). Under the process of radiative transfer, the average distance between donor and acceptor must be larger than the wavelength and the fluorescence lifetime of donors is unchanged [11]. In our system, the inter-dot distance in the dense film is approximately 7 nm. Figure 3.2(c) presents the TRPL spectra of dense and diluted film recorded at 734 nm. The lifetime in the dense film (6.5 ns) is shorter than in the diluted film (40.0 ns). Therefore, the energy red-shift accompanied with the quenching of lifetime of small QDs is evidence of FRET effect between proximal QDs.

The non-radiative energy transfer by dipole-dipole interactions in mono-dispersed CdTe QDs film can be further confirmed by wavelength dependent TRPL measurements. Figure 3.3(a) displays PL spectra of mono-dispersed 5.1 nm CdTe QDs solution ($1.0 \times 10^{-5} M$) and film. Figure 3.3(b) shows the TRPL spectra of mono-dispersed 5.1 nm CdTe QDs film as a function of wavelength (from 670 to 800 nm). A TRPL spectrum of the solution recorded at 734 nm is also displayed in Figure 3.3(b). In order to resolve the time constants, all of the decay curves were analyzed by two PL decay times, the initial (fast) and the slow PL decay time. In Figure 3.3(b), as the dot size increases, the initial PL decay time increase from 2.8 ns (at 670 nm) to 31.0 ns (at 800 nm), indicating the energy transfer from small to large dots right after the initial excitation. However, the slow decay time remains constant (52.0 ns) throughout the whole spectrum range. The decay time of CdTe QDs solution at 734 nm is about 55.0 ns, which is very close to the slow decay time of the film. Due to the large inter-dot distances in the solution, the dipolar coupling effect between adjacent QDs can be neglected. Thus, the decay time origins from the QDs in the absence of energy transfer process. This implies that the slow decay times of the film origin from a subset of CdTe QDs in the film do not participate in energy transfer because of the absence of proximal resonant acceptors [13].

Figure 3.4 shows the instantaneous PL spectra of the mono-dispersed 5.1 nm CdTe

QDs film. After the excitation of the mono-dispersed 5.1 nm CdTe QDs film, the PL emission is peaked at 719 nm. It is identical with the emission from the 5.1 nm CdTe QDs solution. The emission peak shifts to the red rapidly before 20.0 ns and then becomes almost constant at 734 nm after 40.0 ns. Figure 3.5 shows the dynamic red-shift of the PL peak emission of the mono-dispersed 5.1 nm CdTe QDs film. It indicates that all excitons transfer from small to large dots and the transfer process will be suppressed as time passes [13].

The red-shift of PL energy can also be observed in CdTe QDs films with different dot sizes (2.3 nm and 3.4 nm in this study). We found that the amount of PL energy red-shift is independent of CdTe QDs' size but depends on the PL linewidth of the sample. Figure 3.6 plots the PL energy shift (ΔE) versus full width at half maximum (FWHM) of the CdTe QDs. The data are also listed in Table 3.1. Obviously, as the FWHM of the CdTe QDs increases, the PL energy red-shift increases. It suggests that the broader the dot size distribution, the larger the spectral overlap between the emission of small dots and absorption of large dots. [27].



3.2 FRET in Mixed-Size CdTe Colloidal Quantum Dots

In this section, we discuss the mixed-size CdTe QDs films. In Section 3.2.1, a mixture of two different sizes CdTe QDs film will be studied. In Section 3.2.2, the influences of donor to acceptor concentration ratios in mixed-size CdTe QDs films will be discussed.

3.2.1 The Dependence of FRET on Spectral Overlap in Mixed-Size CdTe QDs

Figure 3.7(a) shows absorption and PL spectra of 2.3, 3.4, and 5.1 nm CdTe QDs in aqueous solution at room temperature. To study the mechanism of the FRET, we prepare a mixed solution having 50 % of 3.4 nm dots and 50 % of 5.1 nm dots (with larger spectral overlap) in water. The small (large) dots play of the role of donors (acceptors). Figure 3.7(b) displays the PL spectra of pure donors, pure acceptors, and the mixed films. The PL peak energy for the films exhibits an energy red-shift as compared with that of the solutions. This is because the energy transfer between proximal dots due to QDs' size distribution discussed in Section 3.1. Moreover, we observe that the PL intensity of donors quench and that of acceptors enhance in the mixed film. It is attributable to the electronic energy transfer from donors to acceptors, since the inter-dot distance between donors and acceptors are reduced [14,28].

Further evidences for energy transfer in the mixed film were obtained from TRPL measurements. Figure 3.8(a) shows fluorescence decay curves for the pure donors and mixed films monitored at the peak (635 nm) energy. The decay rate of the mixed film clearly increases with respect to the pure donors. Furthermore, in Figure 3.8(b), the decay rate of the mixed film recorded at peak (734 nm) position decreases with respect to the pure acceptors. The PL decay rate of donors is increased while that of the acceptors is decreased in the mixed film when both the donors and acceptors are excited. The results in the PL (Figure 3.7) and

TRPL (Figure 3.8) spectra are consistent with FRET from donors to acceptors [14,28].

Figure 3.9 shows true-color images of the pure donors, pure acceptors, and mixed CdTe QDs in solutions and films. The images of pure donor (acceptor) QDs in both solution and film exhibit light red (dark red). The image of the mixed QDs solution presents the color between light red and dark red. However, the image of the mixed QDs film displays almost the same color (dark red) with the pure acceptors. It implies that the decrease of the inter-dot distance in the mixed film results in more efficient FRET between donors and acceptors [25].

To have a quantitative understanding of FRET mechanism, we fit the PL decay curves by the bi-exponential function and then obtain the average lifetime of donors [12]. As can be seen in Figure 3.8(a), the lifetime of donors in the mixed film (4.2 ns) is faster than that of pure donors (11.3 ns). The FRET efficiency ($\eta \sim 63\%$) can be calculated using Eq. (5). The value is larger than the FRET efficiency ($\eta \sim 25\%$) of the mixture film of 2.3 and 3.4 nm CdTe QDs. The increased FRET efficiency is mainly attributed to the increase of spectral overlap between donor emission and acceptor absorption, which is listed in Table 3.2. From Eq. (2), the critical distance of FRET (R_0) is calculated to be 5.9 nm which closes to the value of 4.7 nm of CdSe QDs reported previously [14,27]. Using Eq. (4), the inter-dot distance ($R_{DA} \sim 5.5$ nm) between donors and acceptors can also be obtained. The FRET rate γ is 0.15 ns^{-1} and it is calculated by Eq. (1). All of the FRET parameters discussed are shown in the Table 3.2. Our results demonstrate that it is feasible to investigate the influence of inter-dot distance and spectral overlap between donor emission and acceptor absorption on the coupling system by mix two different sizes QDs.

3.2.2 The Dependence of FRET on Donor to Acceptor

Concentration ratios in Mixed-Size CdTe QDs

In this section, we discuss the dependence of FRET on the donor to acceptor concentration ratios (D/A) in the mixed-size CdTe QDs films. Figure 3.10(a) shows the PL spectra of mixed-size CdTe QDs solutions with different donor to acceptor concentration ratios ($D/A = 1, 3, \text{ and } 5$). As the ratio is increased, the PL intensity of donors is strongly enhanced. Slightly increases in PL intensity of acceptors can be assigned to the spectral overlap between the emissions of donors and acceptors. FRET from donors to acceptors in the mixed solution can be ruled out, since no obvious lifetime changes in both donors and acceptors as the ratio increases. Figure 3.10(b) shows the PL spectra of mixed-size CdTe QDs films with different donor to acceptor concentration ratios ($D/A = 1, 3, \text{ and } 5$). In comparison with the experimental results shown in Figure 3.10(a), as the donor increases, the PL intensity of acceptors is significantly enhanced. This indicates that the efficiency of FRET from donors to acceptors is enhanced because acceptors are surrounded by more and more donors [28].

Figure 3.11(a) displays the PL decay curves of donors detected at 635 nm in the mixed CdTe QDs films with different D/A ratios. Figure 3.11(b) displays the PL decay curves of acceptors in the mixed CdTe QDs films with different D/A ratios detected at 734 nm. With an increasing amount of donors, the lifetime of donors (acceptors) in the mixed CdTe QDs film decreases (increases). As can be seen shown in the inset of Figure 3.11(b), the lifetime curves of acceptors in the mixed CdTe QDs films with high D/A ratios exhibit pronounced prolonged excitation during the first few nanoseconds. It is because the magnitude of donor per acceptor is increased and the large number of excitation energy will be transferred from donors to acceptors over first several nanoseconds. The prolonged excitation of acceptors in the mixed films with high D/A ratios must be due to the feeding effect. Moreover, this effect becomes even more pronounced upon recording of the long-wavelength emission. It is remarkable that

the energetic feeding of the acceptors lasts over several nanoseconds, even though the emission of the donors drops within the first nanosecond. Franzl *et al.* reported that excitation energy in small CdTe QDs can be trapped and subsequently be transferred in a stepwise manner to the layer of large QDs [29]. Because the trapped excitations of donors do not contribute to fluorescence, the trapped excitation is not visible in the decay curves of the donors in the mixed film as shown in Figure 3.11(a). However, after the transfer of the trapped excitations to proximal acceptor, the excitations become visible again through the emission from acceptor which is called trapped exciton recycling effect. The simultaneous occurrence of decreasing of the donor decay time and feeding of acceptor decay time provides a strongly evidence of FRET.

Figure 3.12(a) shows the TRPL image of mixed-size CdTe QDs film ($D/A = 5$). Initially after excitation, the donor emission is peaked at 615 nm and the acceptor emission is peaked at 719 nm. Besides, the PL intensity of donors is about three times higher than that of acceptors. As time passes, the PL intensity of donors falls sharply and the emission from acceptors dominates the whole spectrum. Moreover, the PL emission peaks of donors and acceptors shift dramatically towards the low energy side within the first 10.0 ns after excitation. It indicates that the excitons are in the process of energy transfer from small dots to large dots, resulting in the quenching of PL intensity and lifetime of donors as well as an enhancement of acceptors. Beyond 10.0 ns, the emission peak is almost constant at 635 and 734 nm for donors and acceptors, respectively, revealing that all excitons have transferred to large dots and the energy transfer is suppressed. The dynamics of energy transfer can be further depicted by the temporal evolution PL spectra as shown in Figure 3.12(b).

In order to investigate the dependence of FRET on the D/A ratios to an extended range, mixed-size CdTe QDs films with the ratio of 6, 7, 8, and 9 were further studied. Figure 3.13(a) shows the TRPL spectra of donors in mixed-size CdTe QDs films detected at 635 nm for $D/A = 5, 6, 8,$ and 9 . Obviously, when the ratio exceeds 6 and reaches 9, the lifetime of the donor

increases and approaches that of pure donors. Figure 3.13(b) plots the average PL lifetime of donors recorded at peak position in the mixed-size CdTe QDs films as a function of D/A ratios. As the ratio is increased from 1 to 6, the FRET rate is changed from 0.13 to 0.93 ns⁻¹ and the efficiency is changed from 63 to 91 %. This is because acceptors are surrounded by more and more donors. It can be estimated that each acceptor dot is approximately surrounded with six donor dots when the ratio is 6 [25]. However, as the ratio is further increased and reached 9, the lifetimes of donors is increased and approached to that of pure donors. It is because the relative amount of available acceptors is decreased, *i.e.* the donor emission dominates the entire PL spectrum.



Table 3.1 FWHM for 2.3 nm, 3.4 nm, and 5.1 nm CdTe QDs solution, and the amount of red-shift for 2.3 nm, 3.4 nm, and 5.1 nm CdTe QDs film.

Sample	Diameter (nm)	FWHM (meV)	Red-shift (meV)
A	2.3	150	30
B	3.4	210	50
C	5.1	180	40

Table 3.2 Amount of spectra overlap, FRET efficiency, FRET rate, Förster critical radius, and the distance between donor and acceptor for the mixture of two QDs size (3.4 nm + 5.1 nm and 2.3 nm + 3.4 nm).

Sample	Amount of Overlap $J(\omega)$	FRET Efficiency	FRET Rate	Förster Critical Radius	Distance between Donor and Acceptor
		η (%)	γ (ns ⁻¹)	R_0 (nm)	R_{DA} (nm)
3.4 nm + 5.1 nm	5.0×10^{14}	63	0.15	5.9	5.5
2.3 nm + 3.4 nm	1.3×10^{14}	25	0.05	4.7	5.7

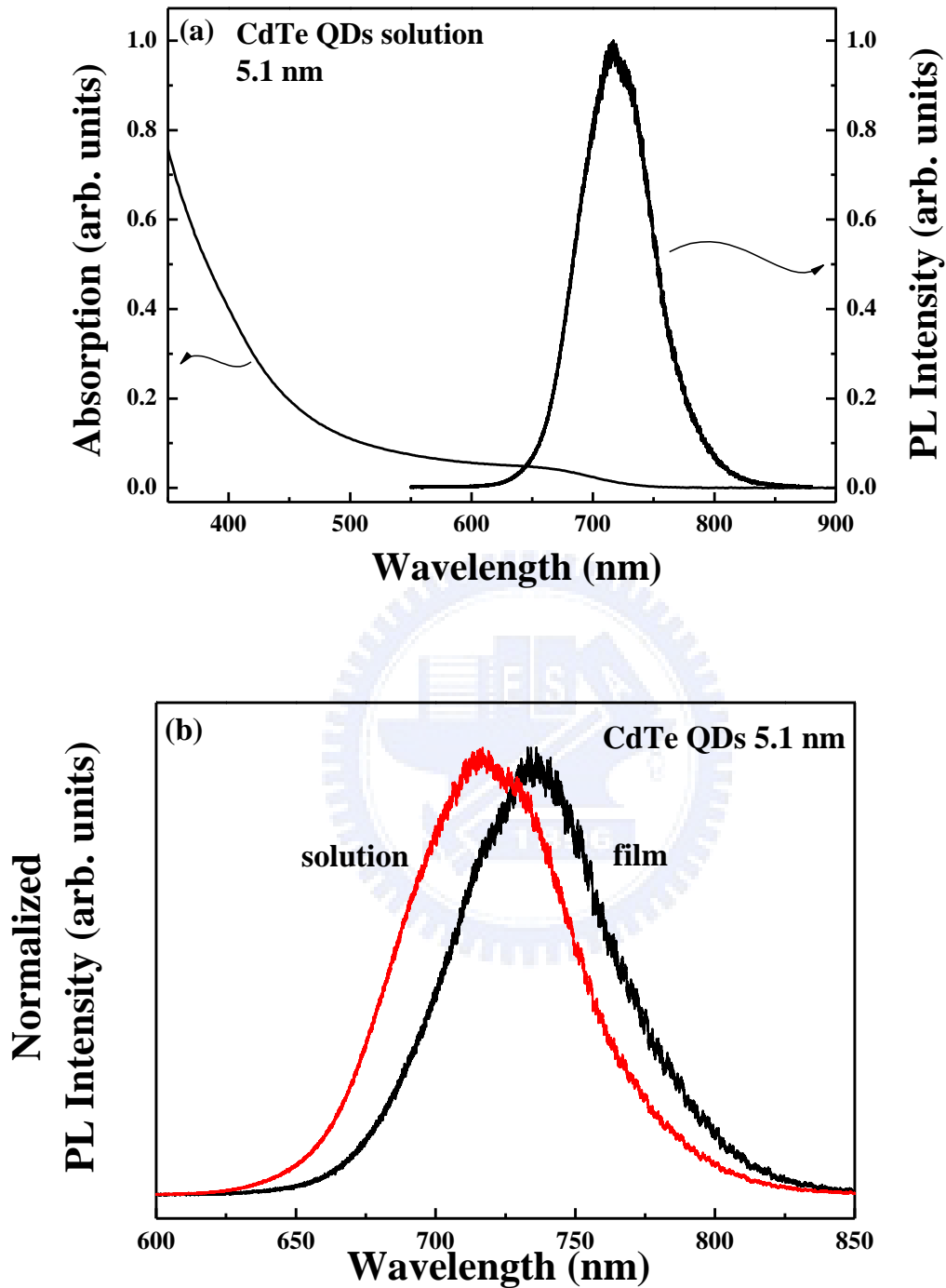


FIG. 3.1. (a) Absorption and normalized PL spectra of mono-dispersed 5.1 nm CdTe QDs solution at room temperature. (b) Normalized PL spectra of 5.1 nm mono-dispersed CdTe QDs solution (red line) and film (black line).

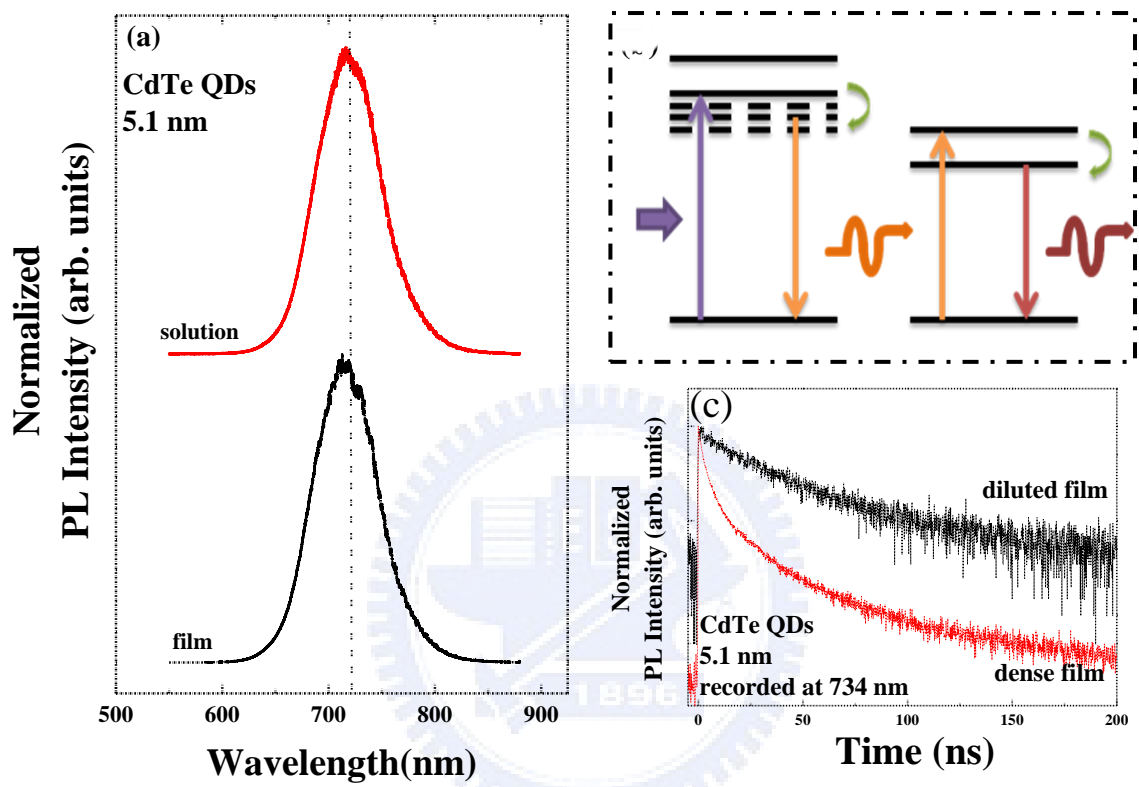


FIG. 3.2. (a) Normalized PL spectra of diluted CdTe QDs solution (red line) and film (black line). (b) Schematic draw of radiative energy transfer. (c) PL decay curves of diluted film (black line) and dense film (red line) measured at 734 nm.

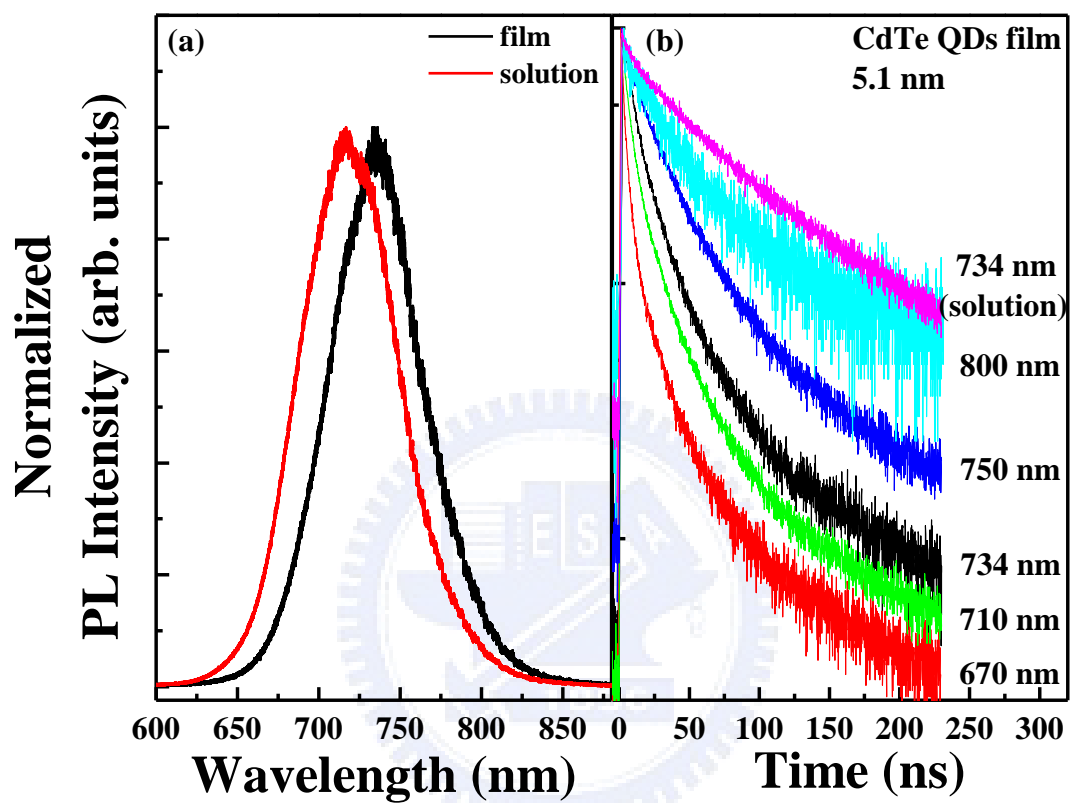


FIG. 3.3. (a) Normalized PL spectra of mono-dispersed 5.1 nm CdTe QDs solution (red line) and film (black line). (b) TRPL spectrum of 5.1 nm CdTe QDs solution recorded at 734 nm is also displayed.

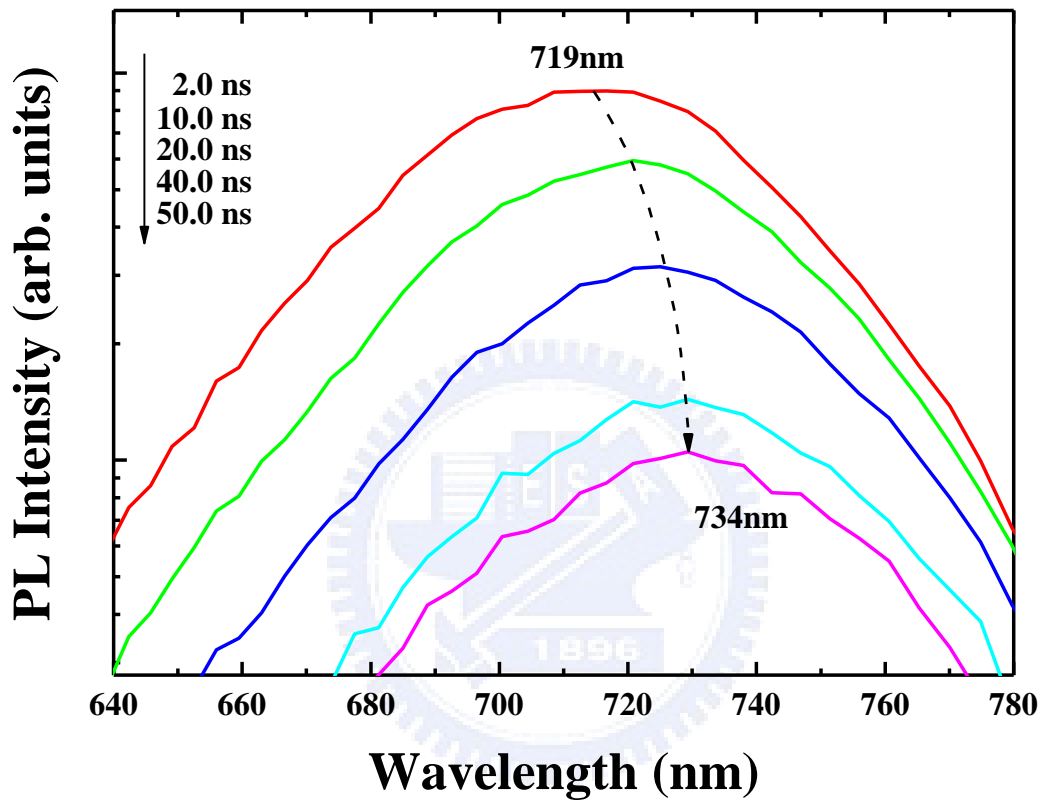


FIG. 3.4. Instantaneous PL spectra of the mono-dispersed 5.1 nm CdTe QDs film.

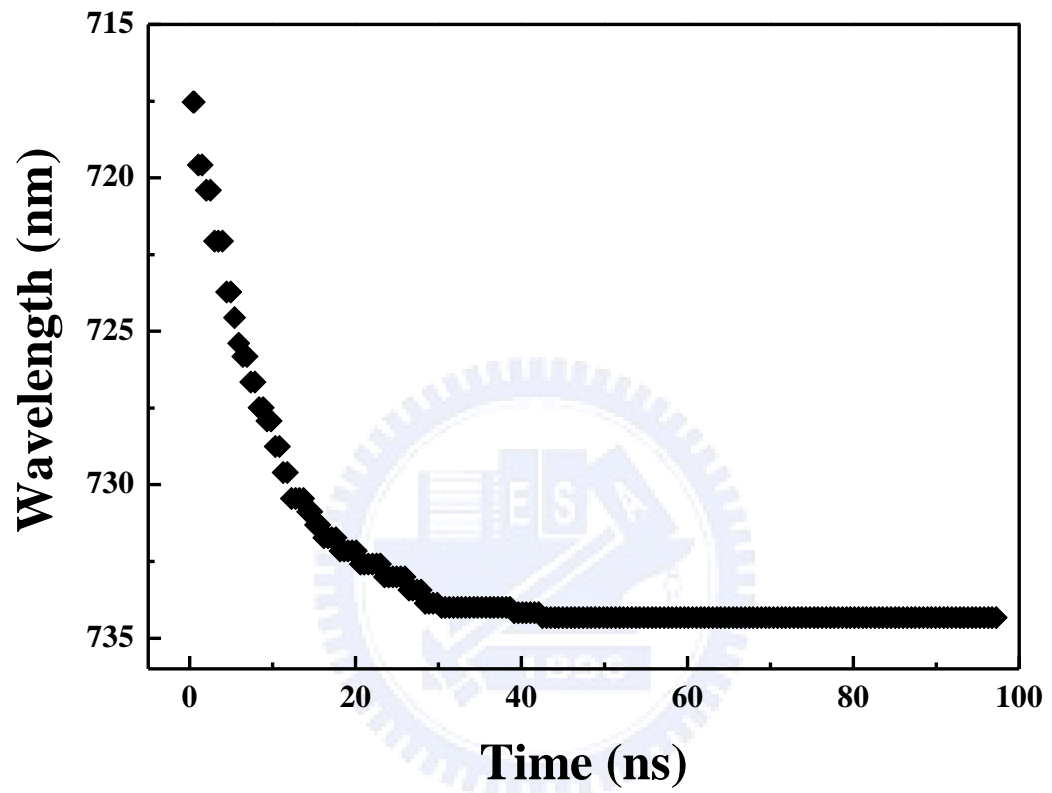


FIG. 3.5. Dynamic red-shift of the PL peak emission of the mono-dispersed 5.1 nm CdTe QDs film.

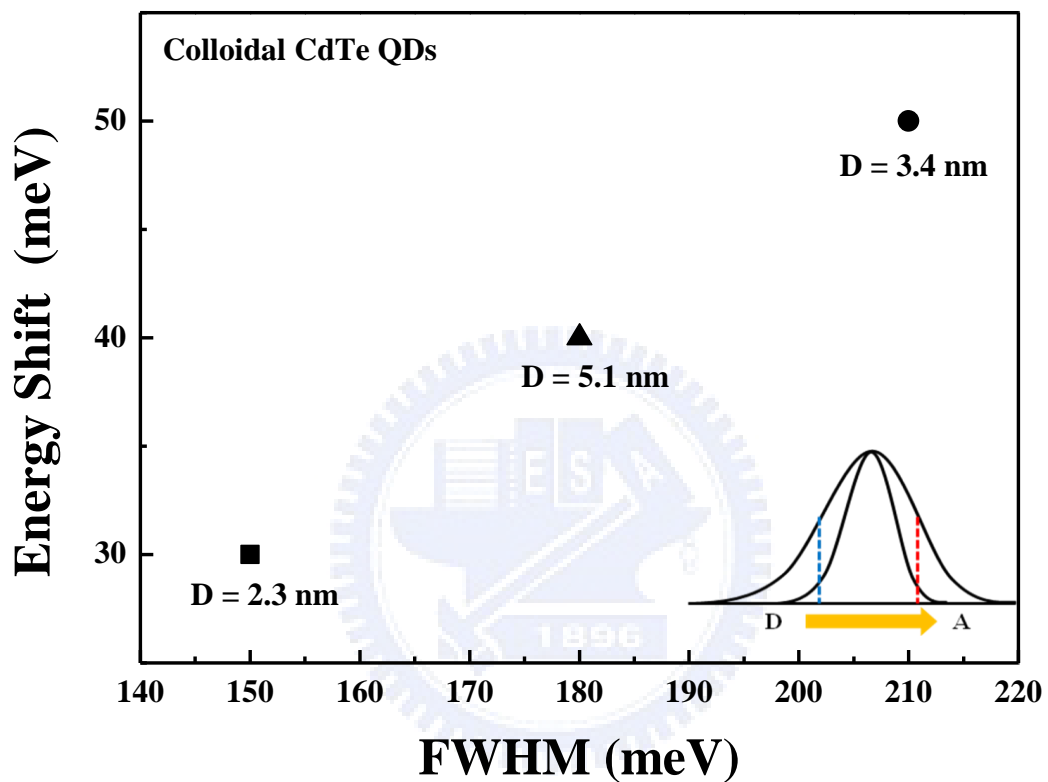


FIG. 3.6. The amount of red-shift versus FWHM for 2.3 nm (square), 3.4 nm (circle), 5.1 nm (triangle) CdTe QDs size.

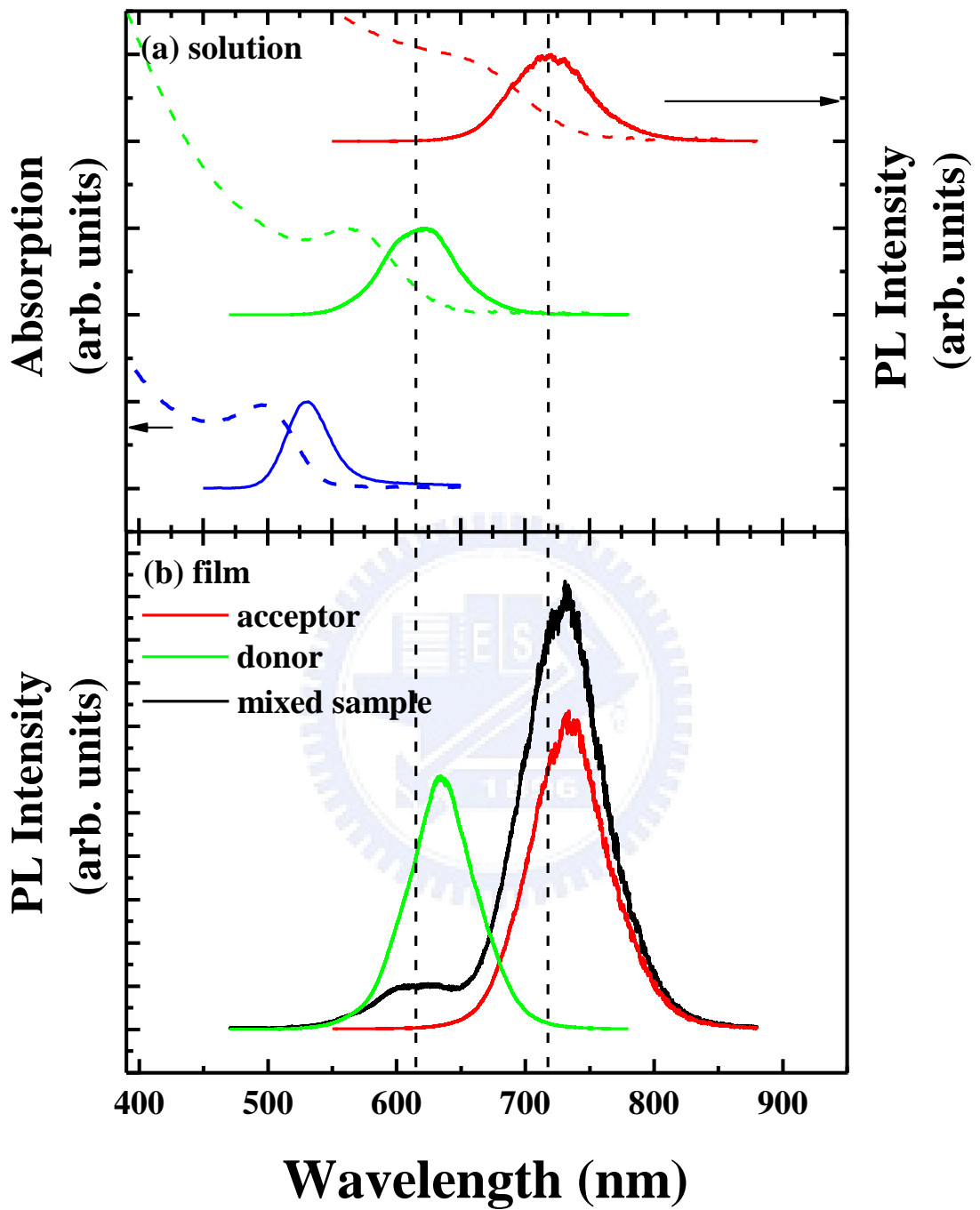


FIG. 3.7. (a) Absorption (dash) and normalized PL spectra (solid) for mono-dispersed 2.3 nm (blue line), 3.4 nm (green line) and 5.1 nm (red line) CdTe QDs solution at room temperature. (b) PL spectra for film of 3.4 nm (green line), 5.1 nm (red line), and mixture of the two (black line).

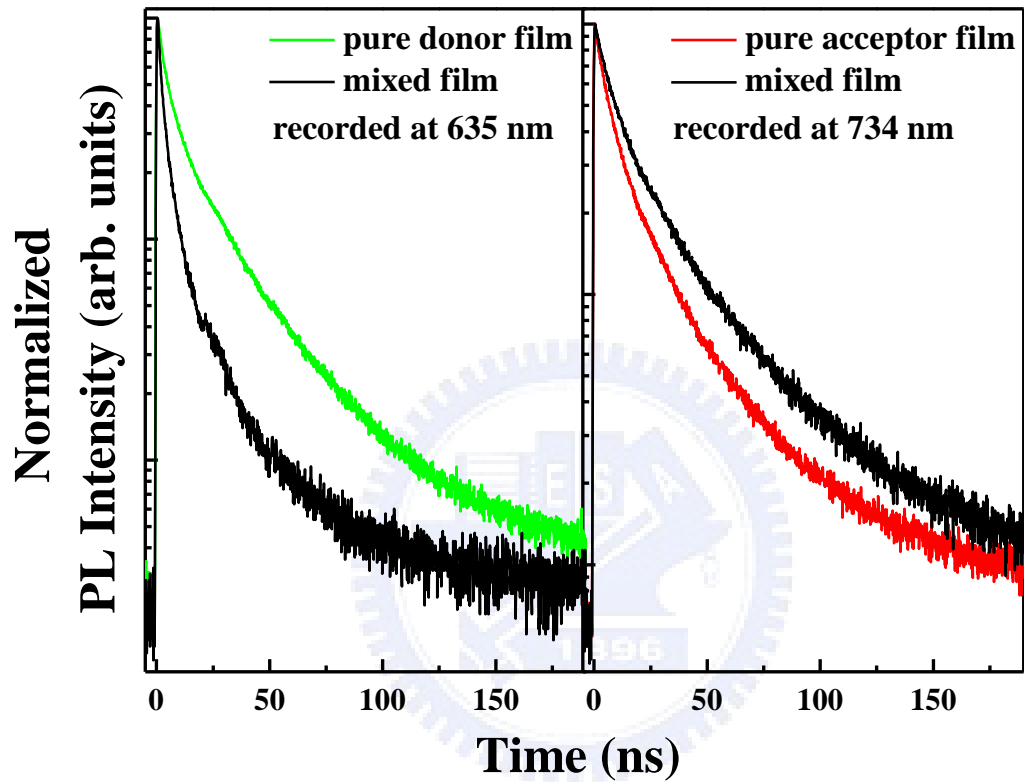


FIG. 3.8. (a) PL decay curves of the pure 3.4 nm CdTe QDs film (green line) and the mixed-size CdTe QDs film (black line) measured at 635 nm. (b) PL decay curves of the pure 5.1 nm CdTe QDs film (red line) and the mixed-size CdTe QDs film (black line) measured at 734 nm.

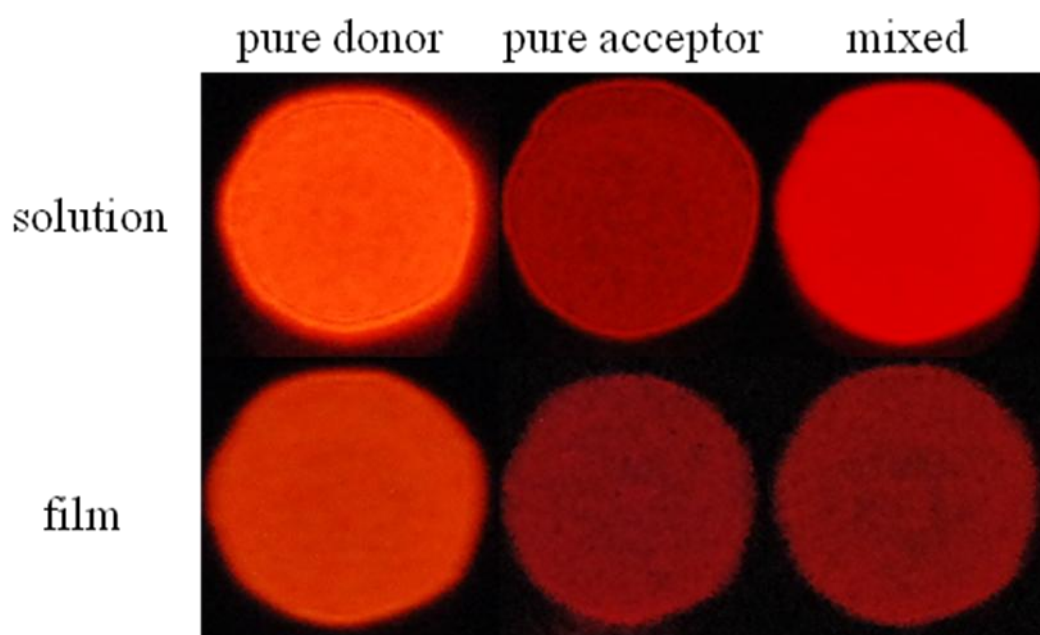


FIG. 3.9. True-color images of the pure donors, pure acceptors, and mixed CdTe QDs in solutions and films.

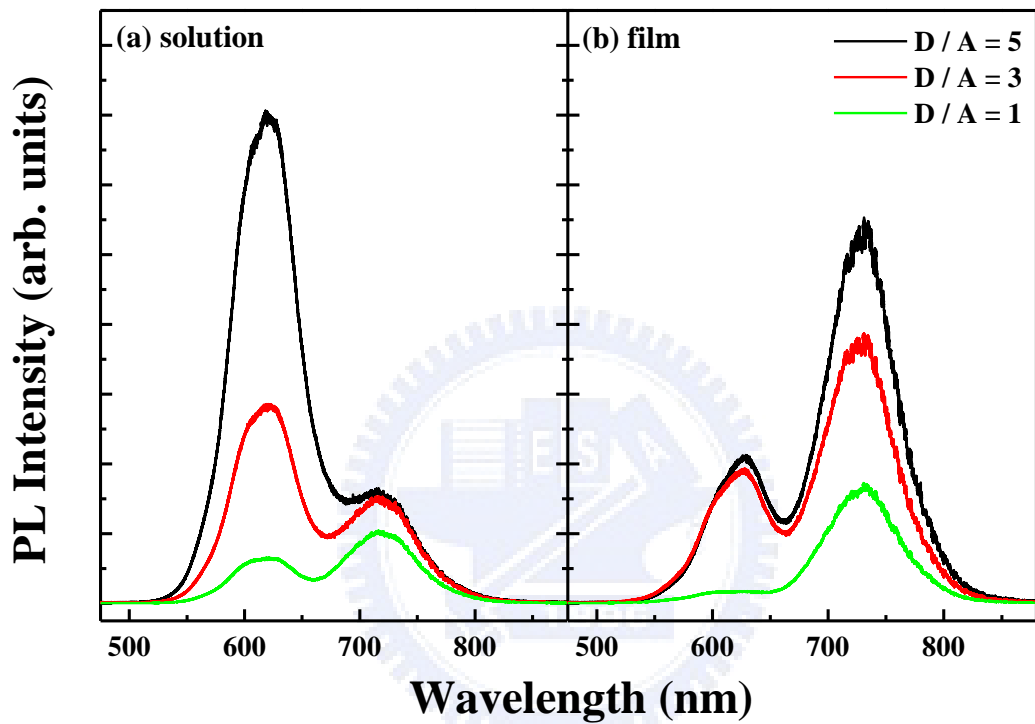


FIG. 3.10. (a) PL spectra of mixed-size CdTe QDs solutions with different donor to acceptor concentration ratios ($D/A = 1, 3,$ and 5). (b) PL spectra of mixed-size CdTe QDs films with different donor to acceptor concentration ratios ($D/A = 1, 3,$ and 5).

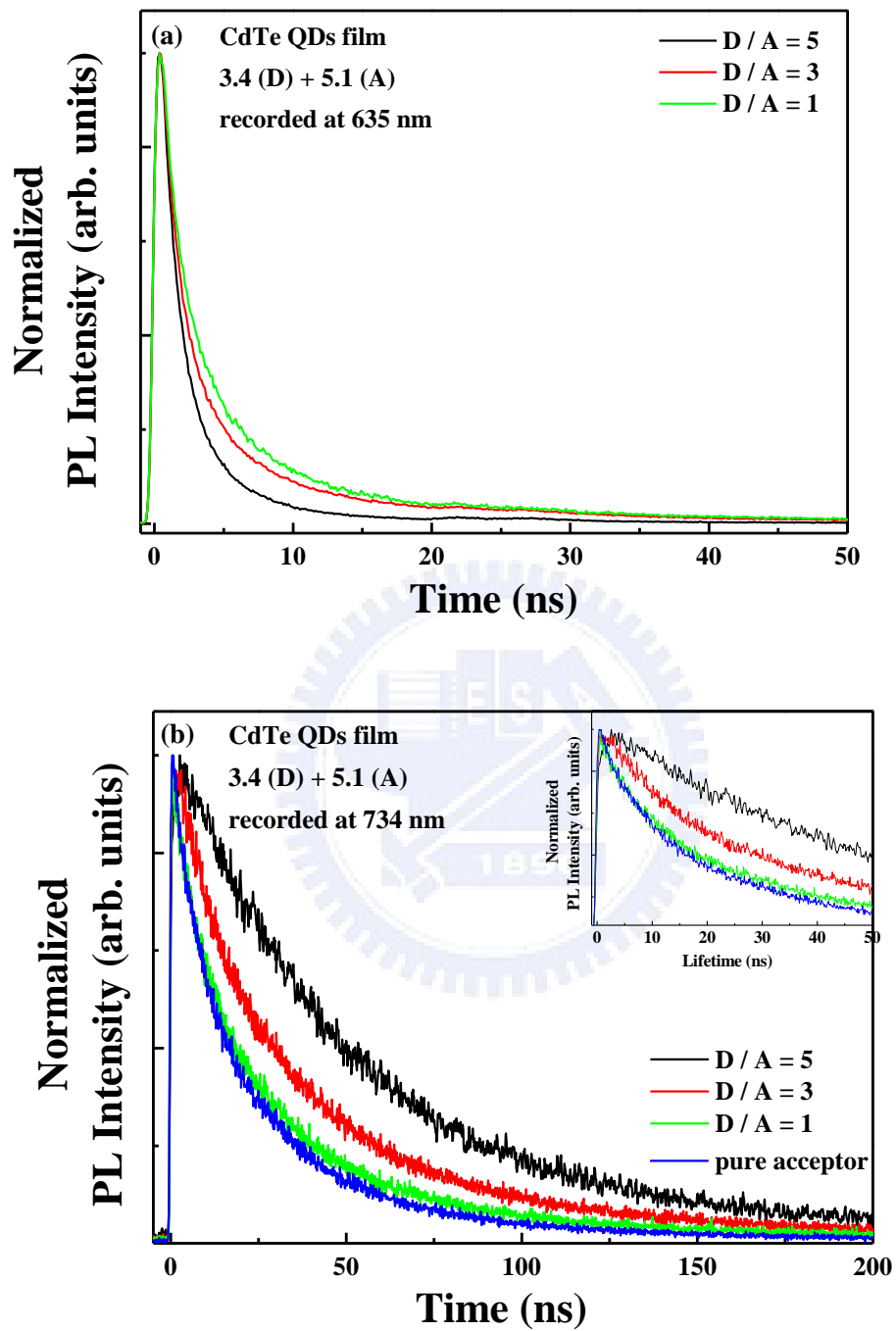


FIG. 3.11. (a) PL decay curves of donors detected at 635 nm in the mixed CdTe QDs films with different D/A ratios. (b) PL decay curves of acceptors detected at 734 nm in the mixed CdTe QDs films with different D/A ratios. The inset shows the initial PL decay curves of acceptors.

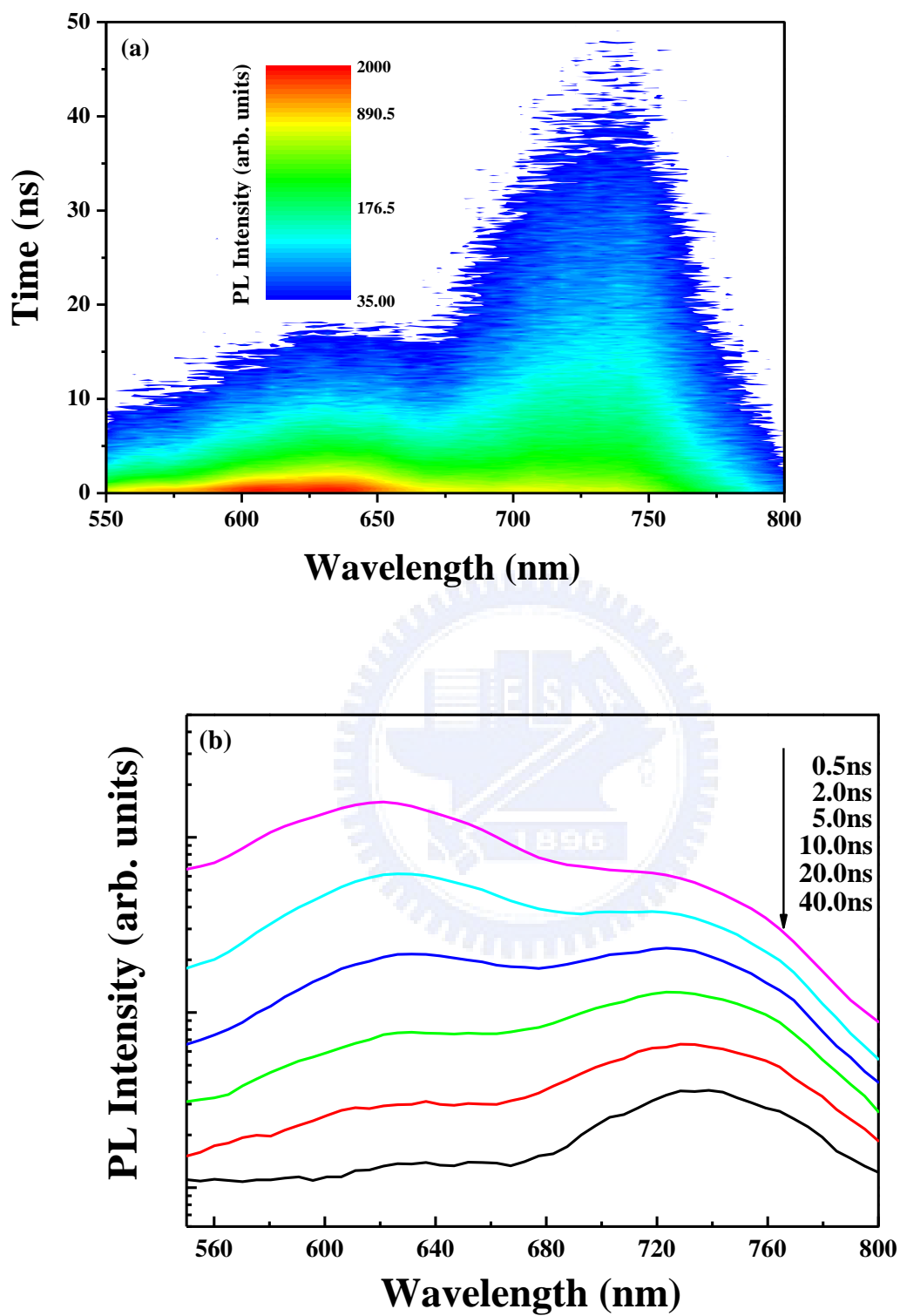


FIG. 3.12. (a) TRPL image of mixed-size CdTe QDs film ($D/A = 5$). (b) Temporal evolution of PL spectra of mixed-size CdTe QDs film ($D/A = 5$).

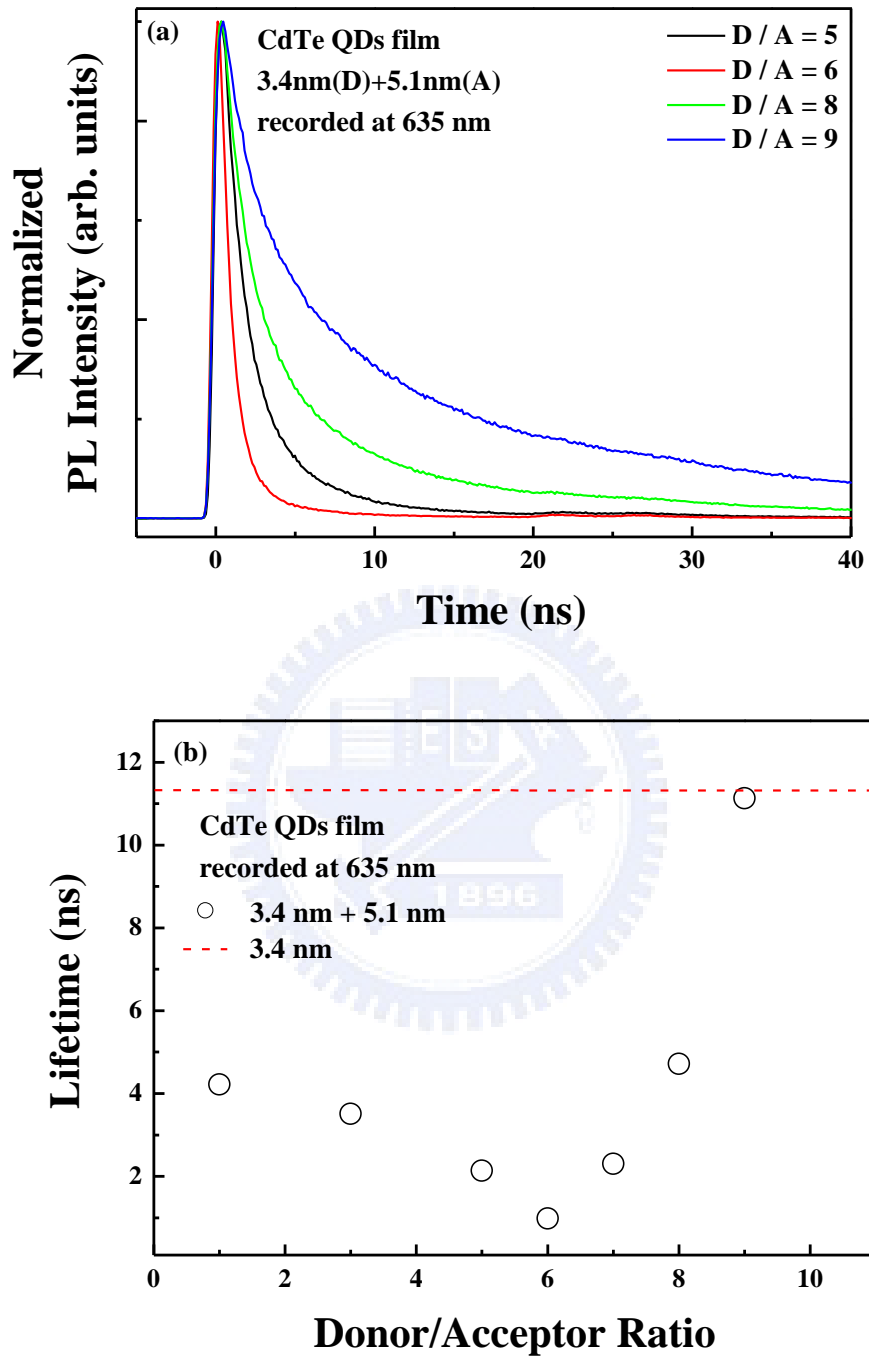


FIG. 3.13. (a) TRPL spectra of donors in mixed-size CdTe QDs films detected at 635 nm for $D/A = 5, 6, 8,$ and 9 . (b) Average PL lifetime of donors (open circles) recorded at peak position in the mixed-size CdTe QDs films as a function of D/A ratios. The PL lifetime of pure donors is also shown (red dash line).

Chapter 4. Conclusions

In conclusion, we demonstrated the FRET dynamics in mono-dispersed and mixed-size CdTe QDs films by using PL and TRPL spectroscopies. A significant PL energy red-shift was observed in mono-dispersed CdTe colloidal QDs films when compared with solutions. The energy dependent TRPL measurements directly reveal the energy transfer from small to large QDs within the sample inhomogeneous distribution. We found that the amount of PL energy red-shift is independent of CdTe QDs' size but depends on the PL linewidth of the sample. The quenching/enhancement of PL intensity and lifetime of donors/acceptors are evidences of FRET effect in mixed-size (50 % 3.4 nm and 50 % 5.1 nm) water-soluble CdTe QDs. Finally, we also found that the donor to acceptor concentration ratio in mixed-size CdTe QDs films is an important parameter, influenced the FRET efficiency. As the ratio is increased from 1 to 6, the FRET rate is changed from 0.13 to 0.93 ns⁻¹ and the efficiency is changed from 63 to 91 %. This is because acceptors are surrounded by more and more donors. However, as the ratio is further increased to 9, the lifetime of donors is approached to that of pure donors. It is because the relative amount of available acceptors is decreased.

References

- [1] A. P. Alivisatos, *Science* **271**, 933 (1996).
- [2] X. Michalet, F. F. Pinaud, L. A. Bentolila, J. M. Tsay, S. Doose, J. J. Li, G. Sundaresan, A. M. Wu, S. S. Gambhir, and S. Weiss, *Science* **307**, 538 (2005).
- [3] Yao He, Li-Man Sai, Hao-Ting Lu, Mei Hu, Wen-Yong Lai, Qu-Li Fan, Lian-Hui Wang, and Wei Huang, *Chem. Mater.* **19**, 359 (2007).
- [4] V. L. Colvin, M. C. Schlamp, and A. P. Alivisatos, *Nature* **370**, 354 (1994).
- [5] Seth Coe, Wing-Keung Woo, Mounqi Bawendi, and Vladimir Bulovic, *Nature* **420**, 800 (2002).
- [6] QingJiang Sun, Y. Andrew Wang, Lin Song Li, DaoYuan Wang, Ting Zhu, Jian Xu, ChunHe Yang, and YongFang Li, *Nature Photonics* **1**, 717 (2007).
- [7] J. M. Caruge, J. E. Halpert, V. Wood, V. Bulović, and M. G. Bawendi, *Nature Photonics* **2**, 247 (2008).
- [8] Alyona Sukhanova, Jérôme Devy, Lydie Venteo, Hervé Kaplan, Mikhail Artemyev, Vladimir Oleinikov, Dmitry Klinov, Michel Pluot, Jacques H. M. Cohen, and Igor Nabiev, *Anal. Biochem.* **324**, 60 (2004).
- [9] Igor L. Medintz, H. Tetsuo Uyeda, Ellen R. Goldman, and Hedi Mattoussi, *Nature Material* **4**, 435 (2005).
- [10] Suparna Sadhu and Amitava Patra, *Appl. Phys. Lett.* **93**, 183104 (2008).

- [11] B. Valeur, *Molecular Fluorescence: Principles and Applications*, (Wiley, New York, 2002).
- [12] Neslihan Cicek, Sedat Nizamoglu, Tuncay Ozel, Evren Mutlugun, Durmus Ugur Karatay, Vladimir Lesnyak, Tobias Otto, Nikolai Gaponik, Alexander Eychmüller, and Hilmi Volkan Demir, *Appl. Phys. Lett.* **94**, 061105 (2009).
- [13] S. A. Crooker, J. A. Hollingsworth, S. Tretiak, and V. I. Klimov, *Phys. Rev. Lett.* **89**, 186802 (2002).
- [14] C. R. Kagan, C. B. Murray, M. Nirmal, and M. G. Bawendi, *Phys. Rev. Lett.* **76**, 1517 (1996).
- [15] T. Franzl, D. S. Koktysh, T. A. Klar, A. L. Rogach, and J. Feldmann, *Appl. Phys. Lett.* **84**, 2904 (2004).
- [16] Marc Achermann, Melissa A. Petruska, Scott A. Crooker, and Victor I. Klimov, *J. Phys. Chem. B*, **107**, 13782 (2003).
- [17] Thomas Franzl, Alexey Shavel, Andrey L. Rogach, Nikolai Gaponik, Thomas A. Klar, Alexander Eychmüller, and Jochen Feldmann, *Small* **1**, 392 (2005).
- [18] Marc Achermann, Melissa A. Petruska, Simon Kos, Darryl L. Smith, Daniel D. Koleske, and Victor I. Klimov, *Nature* **429**, 642 (2004).
- [19] Masaki Kawai, Aishi Yamamoto, Norihiro Matsuura, and Yoshihiko Kanemitsu, *Phys. Rev. B* **78**, 153308 (2008).

- [20] C. W. Chen, C. H. Wang, C. M. Wei, and Y. F. Chen, *Appl. Phys. Lett.* **94**, 071906 (2009).
- [21] C. W. Chen, C. H. Wang, Y. F. Chen, C. W. Lai, and P. T. Chou, *Appl. Phys. Lett.* **92**, 051906 (2008).
- [22] Akihiro Ueda, Takeshi Tayagaki, and Yoshihiko Kanemitsui, *Appl. Phys. Lett.* **92**, 133118 (2008).
- [23] Teresa Pellegrino, Liberato Manna, Stefan Kudera, Tim Liedl, Dmitry Koktysh, Andrey L. Rogach, Simon Keller, Joachim Rädler, Giovanni Natile, and Wolfgang J. Parak, *Nano Lett.* **4**, 703 (2004).
- [24] Daniele Gerion, Fabien Pinaud, Shara C. Williams, Wolfgang J. Parak, Daniela Zanchet, Shimon Weiss, and A. Paul Alivisatos, *J. Phys. Chem. B* **105**, 8861 (2001).
- [25] Ling Xu, Jun Xu, Zhongyuan Ma, Wei Li, Xinfan Huang, and Kunji Chen, *Appl. Phys. Lett.* **89**, 033121 (2006).
- [26] Ling Xu, Jun Xu, Wei Li, Zhao Weiming, Ping Sun, Zhongyuan Ma, Xinfan Huang, and Kunji Chen, *J. Mater. Sci.* **42**, 9696 (2007).
- [27] C. R. Kagan, C. B. Murray, and M. G. Bawendi, *Phys. Rev. B* **54**, 8633 (1996).
- [28] Sergiy Mayilo, Jan Hilhorst, Andrei S. Susha, Cornelia Höhl, Thomas Franzl, Thomas A. Klar, Andrey L. Rogach, and Jochen Feldmann, *J. Phys. Chem. C* **112**, 14589 (2008).
- [29] Thomas Franzl, Thomas A. Klar, Stefan Schietinger, Andrey L. Rogach, and Jochen

Feldmann, Nano Lett. **4**, 1599 (2004).

